Translational Oncology
www.transonc.com

Volume 9 Number 3 June 2016 pp. 179–183 179

Scanning Acoustic Microscopy—A Novel Noninvasive Method to Determine Tumor Interstitial Fluid Pressure in a Xenograft Tumor Model[1]

Matthias Hofmann*,[2], Ralph Pflanzer*,[2], Anowarul Habib[†,‡], Amit Shelke[§], Jürgen Bereiter-Hahn[‡], August Bernd*, Roland Kaufmann*, Robert Sader[¶] and Stefan Kippenberger*

*Department of Dermatology, Venereology and Allergology, Goethe University Frankfurt, 60590, Frankfurt am Main, Germany; [†]Dept. of Physics and Technology, University of Tromsø, 9037, Tromsø, Norway; [‡]Institute for Cell Biology and Neurosciences, Goethe University Frankfurt, 60439, Frankfurt am Main, Germany; [§]Department of Civil Engineering, Indian Institute of Technology, Guwahati, India; [¶]Department of Oral, Craniomaxillofacial and Facial Plastic Surgery, Goethe University Frankfurt, 60590, Frankfurt am Main, Germany

Abstract

Elevated tumor interstitial fluid pressure (TIFP) is a prominent feature of solid tumors and hampers the transmigration of therapeutic macromolecules, for example, large monoclonal antibodies, from tumor-supplying vessels into the tumor interstitium. TIFP values of up to 40 mm Hg have been measured in experimental solid tumors using two conventional invasive techniques: the wick-in-needle and the micropuncture technique. We propose a novel noninvasive method of determining TIFP via ultrasonic investigation with scanning acoustic microscopy at 30-MHz frequency. In our experimental setup, we observed for the impedance fluctuations in the outer tumor hull of A431-vulva carcinoma–derived tumor xenograft mice. The gain dependence of signal strength was quantified, and the relaxation of tissue was calibrated with simultaneous hydrostatic pressure measurements. Signal patterns from the acoustical images were translated into TIFP curves, and a putative saturation effect was found for tumor pressures larger than 3 mm Hg. This is the first noninvasive approach to determine TIFP values in tumors. This technique can provide a potentially promising noninvasive assessment of TIFP and, therefore, can be used to determine the TIFP before treatment approach as well to measure therapeutic efficacy highlighted by lowered TFP values.

Translational Oncology (2016) 9, 179–183

Introduction

Elevated tumor interstitial fluid pressure (TIFP), as already shown in the early works of Young et al. in the 1950s, has been identified as a major barrier for transmigration of larger molecules into the interior of solid tumors [1]. TIFP is outwardly directed and hampers mainly the transport of big molecules as they are dependent on convectional flow rather than diffusional effects [2–4]. Moreover, a heightened TIFP not only has significant effects on molecular transport but also plays a role in inducing mechanical stress on the tumor capsule, thereby triggering cell proliferation; in turn, the lowering of TIFP accounts for beneficial effects on tumor progression [5,6]. Measuring

Address all correspondence to: Matthias Hofmann, PhD, Department of Dermatology, Venereology and Allergology, Goethe University Frankfurt, Theodor-Stern-Kai 7, 60590, Frankfurt am Main, Germany.
E-mail: matthias.hofmann@em.uni-frankfurt.de

[1] This work has been supported by the LOEWE Praebionic Network (BOSS4 to R.P. and M.H., BOSS6 to R.S., and Me2 to A.S.) and the Harry und Rosa Neumann Foundation (to M.H.).

[2] These authors contributed equally to this work.

Received 30 December 2015; Revised 25 March 2016; Accepted 30 March 2016

1936-5233/16
http://dx.doi.org/10.1016/j.tranon.2016.03.009

the TIFP has been performed by invasive, hydrostatically coupled techniques such as the wick-in-needle or the micropuncture method [7,8].

Still, nowadays, one of the biggest problems in tumor therapy is how to effectively transport high-molecular substances like monoclonal antibodies to its desired target location. The knowledge of the TIFP as a "physical biomarker" to presume the efficacy of drug uptake would help the clinicians to determine tumor therapies. Therefore, it is desirable for future clinical and preclinical applications to develop a noninvasive measuring method which relies on merely acoustic signal acquisition. Multiple tissues have been characterized with high-frequency acoustic techniques to quantify the biomechanical properties of cells and internal cellular structures in the past years [9,10]. In regard to biophysical effects of TIFP, our group has employed scanning acoustic microscopy (SAM) in an early stage of development to measure TIFP values [11]. In a recent work, we proposed SAM as a putative method of choice for the noninvasive investigation of TIFP using an improved setup to measure TIFP.

Material and Methods

Cell Culture and Drugs

A431 epidermoid vulva carcinoma cell line was purchased from the American Type Culture Collection (ATCC/LCSC Standards, Wesel Germany) and cultured in low-glucose Dulbecco's modified Eagle's medium (Invitrogen, Karlsruhe, Germany) containing 10% fetal calf serum (Gibco, Paisley, UK). Cells were cultured for several days or a few weeks until a density of 12×10^7 cells per 25-ml flask was reached. After trypsin/EDTA (Gibco, Paisley, UK) treatment, cells were harvested and centrifuged. Cells were then subcutaneously injected into immune-suppressed mice (see below) at a density of 5×10^6 cells per flank.

Tumor Models

For the required tumors to grow, female Naval Medical Research Institute nude mice (5-6 weeks, 18-22 g; Janvier Labs, Le Genest-Saint-Isle, France) were subcutaneously injected on both flanks with 5×10^6 A431 cells. The animals were kept in a pathogen-free environment, and the experiments were approved in accordance with the German animal welfare regulations (Regierungspräsidium Darmstadt, FK/1002). The mice had access to sterilized food and tap water *ad libitum*. For quick *in situ* tumor volume measurements, anesthesia was carried out under isoflurane (Forene, Abbott, Wiesbaden, Germany) vaporizer stream (2%). For tumor excision, ketamine/xylazine (100/10 mg/kg, intraperitoneally; Pharmacia, Erlangen, BayerVet, Leverkusen, Germany) injections were applied. Tumor excision was performed when a size no larger than 20% of the total body weight of mice was reached individually. After excision, anesthetized mice were sacrificed.

Phantom Models and TIFP Measurements

Phantom models were established using balloon and Fogarty thrombectomy catheters (320808 F, Edwards Lifesciences, Unterschleißheim, Germany) as spherical/ellipsoid reflectors of 13 mm diameter and maximum liquid capacity of 2.25 ml 0.9% NaCl solution (B. Braun, Melsungen, Germany).

For simultaneous, invasive calibration measurements of TIFP, a digital pressure transducer including digital amplifier TAM-D (Hugo-Sachs-Elektronik, Harvard Apparatus GmbH, March-Hugstetten, Germany) was used. In the tumors, the cannulae (size 27G) were injected instantaneously via a proprietary spring-controlled injection system which was hydrostatically coupled to the pressure transducer and amplifier. *Aqua dest.* respectively 0.9% NaCl solution were used as coupling fluids and heated up to a stable temperature of 37°C (±0.1°C accuracy) via a P.I.D. controlled heating system (Watlow GmbH, Kronau, Germany). A self-developed vacuum fixation device with a pump flow rate of 3 l/h at 20 rpm was used to keep the submersed tumors immovable. For measurement, excised tumors were put in a cone-shaped Perspex holder with a filter-covered bottom outlet (Ø 5 mm) for the vacuum pump.

Acoustic Microscopy

Scanning acoustic microscopes (SAM 100/AM300, PVATePla, Aalen, Germany), equipped with variable detachable transducers, were used. The piezoelectric transducer, which yielded optimal compromise between penetration depth and resolution, had a center resonating frequency of 30 MHz and was comprised of ZnO with a sapphire backing lens with half opening angle at 30°, focusing with a lateral resolution of 20 µm. The signal has a bandwidth of 30 MHz @ 2 dB and was sampled with a resolution of 8 bits at 500 MS/s prior to storage on the microscope internal hard drive. The radiofrequency output gain curve was determined on a 13-mm-diameter phantom model and subsequently adjusted at a fixed value throughout the experiments to obtain good topological imaging without increasing systematic noise. The typical acquisition time was set for C-scan at 40 seconds in an imaging mode with 500 × 500 pixels.

Image Acquisition and Image Analysis

Images were acquired in B- and C-operational modes of the acoustic microscope with Windows-based software (WinSam) at given maximum *x-y* resolution. Image data were stored in SAM and TIFF data output formats and analyzed by SAMnalysis software 2.1 (PVATePla, Aalen, Germany) and Image-J (NIH, Bethesda, MD).

Results

To show the feasibility of extracting intensity and contrast information changes out of B- and C-mode sonographic images, the complex echogenic situation in a real three-dimensional tumor was reduced to a simplified phantom model system. A fluid-filled balloon and Fogarty thrombectomy catheter system with stepwise-controllable inflation/deflation operation modes were used. Internal

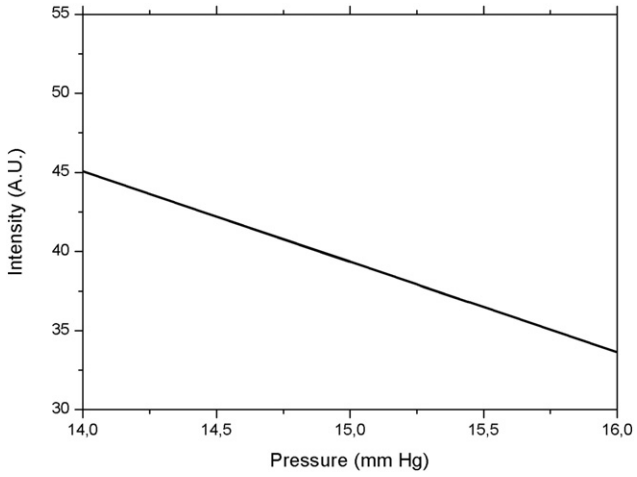

Figure 1. Graph displaying the relationship between hydrostatically recorded TIFP values and obtained B-mode image gray value intensity for the hull of a 13-mm balloon catheter phantom model.

pressure was measured hydrostatically and followed simultaneously with consecutive B-mode imaging in the AM300. Upon *z*-axis (focus)–compensated signal acquisition and during deflation, a linear drop in signal intensity strength could be observed for the peak position of the outer phantom model hull, as displayed in Figure 1. The exemplary graph indicates, consequently, that a stepwise rise of 2 mm Hg in fluid pressure is accompanied by a linear approximate decrease of 10 AU mean signal intensity, while keeping all other physical parameters (temperature, movement, external fluid pressure) constant throughout the measurement.

As SAM converts the received integrated back-reflected ultrasonic wave patterns into visible images, consisting of gray-scaled pixels of varying intensity, the signal strength can be triggered and electronically enhanced with setting the gain. To account for the user- and/or device-dependent signal influence, gain-intensity calibration graphs were taken (Figure 2). The graph indicates a device-specific rise of signal amplitude with increase of electronic gain, leveling off after increasing gain over 30 dB strength. An optimal peak window of 26-28 dB gain was thus determined for setting constant gain in further investigations.

After completing phantom model measurements, excised A431 tumors of comparable size (21 × 12 mm) and with sphere- or elliptical-shaped morphology were investigated with 30 MHz under the acoustic microscope in two states: first in "normal," pressurized condition and, second, after release of 3 mm Hg of pressure by inserting a 27G cannula for hydrostatic calibration measurement. For this purpose, a spring-controlled needle insertion system injected the cannula into the tissue within a time frame of less than 0.5 second. Figure 3 displays the setup and results of lateral C-mode imaging as well as obtained intensity distribution changes for both states. The excised and fixed A431 tumor can be seen in an all-max projected C-scan image consisting of a stack of 250-µm step-sized images between 750 and 3050 µm *z*-axis focal depth (Figure 3*a*). The same tumor is depicted in the depressurized state (Figure 3*b*); arrows indicate major changes in the structural architecture of the tumor hull and the entry point of the cannula. The resulting redistribution of the intensity signal can be seen in Figure 3, *c* and *d*, where the intensity signals are displayed in relation to their pixel position in *x*-direction on a cross-cut line 288 pixels reduced from top. In Figure 3*d*, the two signal intensity peaks within the 300-pixel region show a downshift of 52 and 8 AU, respectively, when compared with the corresponding peaks in Figure 3*c*. The third major peak, located in the right outermost tumor rim region (at an *x*-value of 450 pixels), exhibits an upshift of 20 AU.

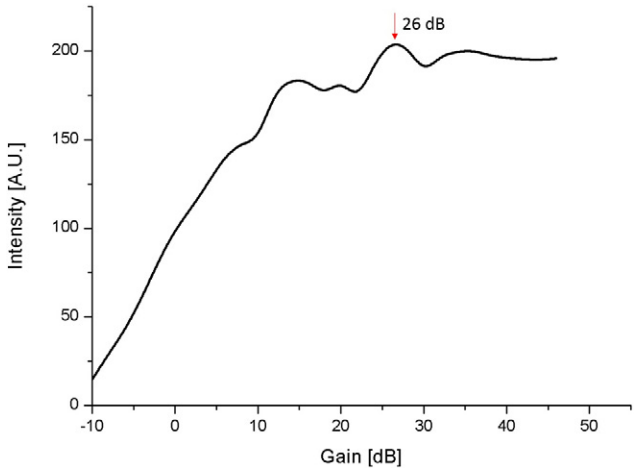

Figure 2. Intensity distribution of B-mode images from a balloon catheter phantom model is depicted dependent of the electronic gain setting. Peak optimal setting is indicated by an arrow.

Corroborating these results, Table 1 gives an overview over obtained mean gray value intensity changes before and after pressure release, when integrated with the white dashed boundaries outlined in Figure 3, *a* and *b*. The mean intensity decreases from 83 to 79 AU within a constant region of interest (ROI). The third row indicates an intermittent value (81 AU) in case the ROI is adjusted to the slightly altered lateral tumor shape.

In addition, we performed B- and C-scan analysis of tumor samples using a lower frequency of 10 MHz. Supplemental Figure 1 shows a 10-MHz sonographic B-scan image of an A431 tumor. The figure highlights that this resolution does only exhibit a rough outline of the tumor rim with speckled gray value distribution and low contrast areas. Therefore, we determined not to use frequencies below 30 MHz for further measurements. On the other hand, higher frequencies above 30 MHz do not yield enough spatial resolution (8-9 mm) even for subsurface tumors.

In the following experiments, intensity distributions in B-mode images of the rim of excised A431 tumors have been analyzed accordingly for a state of normal and one of decreased pressure (data not shown). Simultaneously, hydrostatic pressure measurements have been carried out via the TAM-D, resulting in a graph displaying gray value intensity dependent of tumor pressure, as indicated in Figure 4. In a limited set of six cases of A431 tumors, tumor pressures over 3 mm Hg were not resolvable anymore in terms of intensity increase. After quasilinear signal increase, asymptotic saturation of signals in the range of 11 AU can be observed.

Discussion

The necessity for a noninvasive, nondestructive means of determining biophysical properties of tissue, especially tumor tissue, makes ultrasound microscopy in midfrequency ranges of 30 MHz the method of choice in our experiments. Higher frequencies, e.g., in the gigahertz spectrum, with improved resolution are only applicable to thinner structures such as living cells and cell components and were commonly used before [12]. Low-resolution ultrasound with higher penetration depths, in turn, is regularly applied in medical ultrasound applications, e.g., for tumor volume determination [13].

Our investigation focused on flexible phantom models as a system reduced in complexity because ultrasound waves encounter not only material-specific attenuation but also scattering and small-scale impedance changes within real inhomogeneous biological tissue. As Figures 1 and 2 indicate, a linear reciprocal relationship between intensity in lateral B-mode images and phantom model pressure could be established for the outer rim. Hompland et al. (2012) showed that elevated IFP is uniformly elevated in experimental tumors from the tumor center until the tumor rim [14]. This indication and the assumption that major stress tension is loaded on the outer hull of the tumor, in turn influencing acoustic density, focused our later investigation on the boundaries of the A431 tumors as well. The connection to the microenvironment of the tumor is also mediated over this boundary and includes extravasation and lymphatic drainage

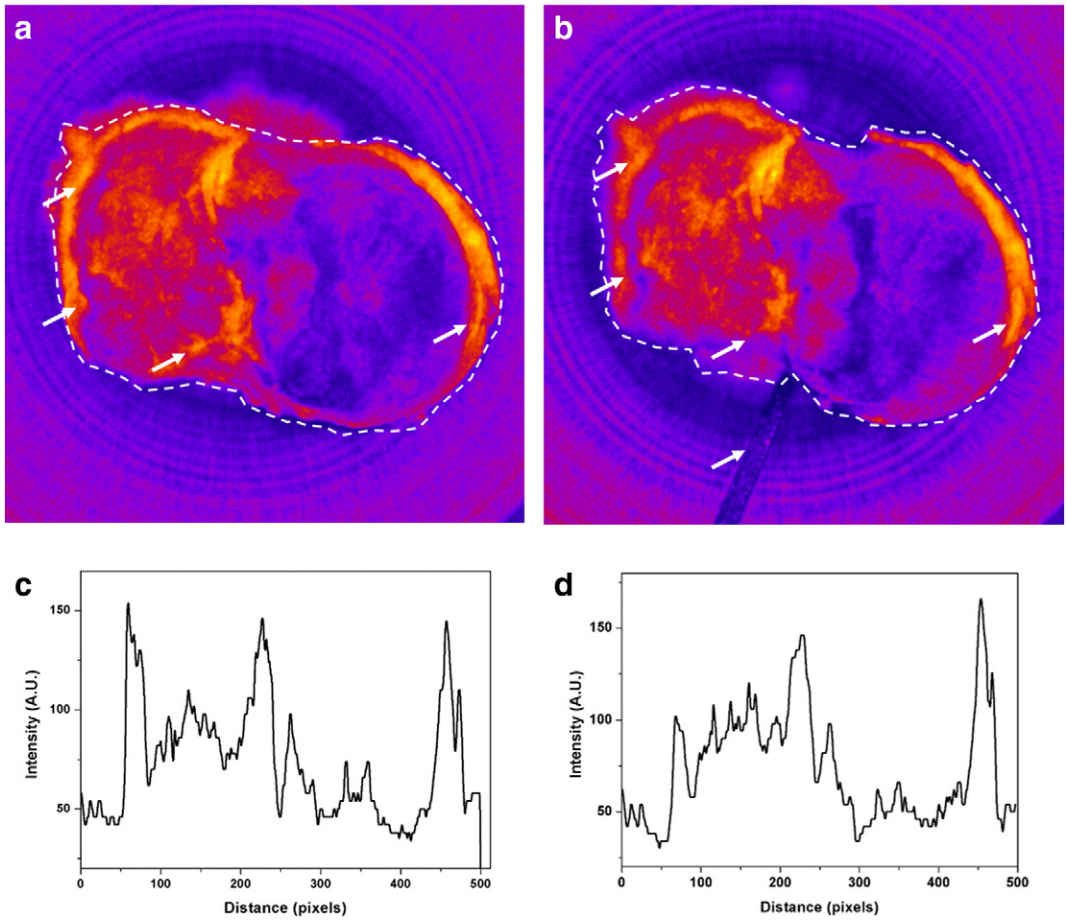

Figure 3. An excised A431 tumor imaged with 30 MHz in SAM. (A) A431 tumor in an all-max projection stack of C-scan images in natural, "pressurized" state. (B) The same tumor after measuring TIFP and a release of 3 mm Hg of pressure. White dashed area in both pictures indicates ROI taken for mean density determination. White arrows indicate major areas of signal redistribution and entry point of the 27G cannula. (C) Intensity profile distribution for a lateral cross-cut line through the C-scan image (288 pixels from top) in pressurized state. (D) Intensity profile distribution for the same cross-cut line after release of 3 mm Hg of pressure.

effects in a real-world tumor setup as well as in a mathematical model of IFP [15]. In a simplified setup with excised solid tumors, fixed for manipulation-free handling and calibrated to a simultaneous, instantaneous hydrostatic IFP measurement, the described method is able to record B- and C-mode images for two states of these tumors: one with normalized pressure and one with a pressure release of 3 mm Hg up to 9 mm Hg. For the 3–mm Hg A431 tumor, we could show a redistribution of acoustic signal in C-scan analysis. Mean intensity was considerably decreased (from 83 to 79 AU) as Table 1 indicates, and peak intensities at left boundaries decreased as well, as displayed in Figure 3, *c* and *d*. However, an increase of signal strength for the right boundary could be observed which might be attributed to compartmentalization of this tumor. Finally, first measurements on a subset of six experimental tumors with internal fluid pressures between 1 and 9 mm Hg show that, for measured values over 3 mm

Table 1. Table Indicating Size of the Tumor ROI; Mean Intensities Determined from the C-Scan Images in Figure 3, *a* and *b*; and Minimum and Maximum Brightness Distribution in the ROIs

A431 tumor conditions	Area (total pixel count)	Mean intensity (AU)	Min (AU)	Max (AU)
TIFP state (pressurized)	103,059	82.994	26	202
3 mm Hg of pressure release	103,059	79.422	22	218
After release, resized ROI	98,574	81.148	22	218

Values are calculated for three cases: basic pressurized state of the tumor, after release of 3 mm Hg of pressure, and for the same release with fitting the ROI to the slightly altered tumor shape.

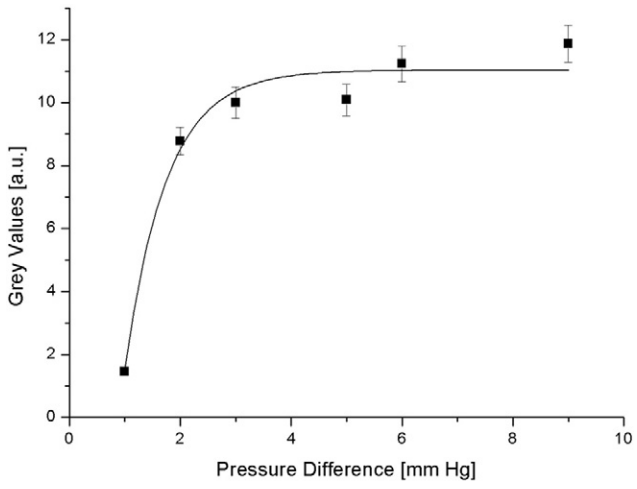

Figure 4. Asymptotic fit plotted for the gray value intensity distribution in relationship to the hydrostatically determined TIFP in a set of six excised A431 tumors, imaged with 30-MHz SAM.

Hg, the intensity curve converges to a maximum of 11 AU. Further increase of TIFP seems not to yield higher values than this cutoff border. This is an effect which cannot be attributed to signal overdrive because Table 1 also indicates that the maximum of 256 bits gray value signal maximum intensity has not been reached. Larger studies into the effects of how acoustic density and number of scatterers influence the distribution and integration of intensity signals in image processing have to follow to investigate this effect, similar to the analysis methods for breast cancer parametric images [16].

Conclusion

In this paper, we propose a novel, noninvasive method of assessing TIFP in experimental solid tumors via SAM at 30 MHz. Once calibration to the conventional pressure measurement method via a fluid-filled capillary has been carried out, changes in ultrasound signal intensity did—with given constant environmental parameters—correspond to changes in internal fluid pressure. We can show that, in case of phantom models and in an excised A431 tumor xenograft model, these signal changes can be tracked and quantified in a limited range of pressure values. However, the technical setup to keep remaining physical parameters uninfluenced (tumor movement, temperature, deformation by needle insertion) is extensive. Nonetheless, improvements in fixation and measuring speed could overcome this in the future, and a potential application to *in situ* measurements of xenograft tumors would put this method in the focus for preclinical application, e.g., to study the effects of lowering TIFP first before applying chemotherapy.

Supplementary data to this article can be found online at http://dx.doi.org/10.1016/j.tranon.2016.03.009.

Conflict of Interest Statement

The authors of this paper report no financial or other conflict of interest relevant to the subject of this article.

Acknowledgements

This work has been supported by the LOEWE Praebionic Network (BOSS4 to R.P. and M.H., BOSS6 to R.S., and Me2 to A.S.) and the Harry und Rosa Neumann Foundation (to M.H.).

References

[1] Young JS, Lumsden CE, and Stalker AL (1950). The significance of the tissue pressure of normal testicular and of neoplastic (Brown-Pearce carcinoma) tissue in rabbits. *J Pathol Bacteriol* **62**, 313–333.

[2] Baxter LT and Jain RK (1989). Transport of fluid and macromolecules in tumors. I. Role of interstitial pressure and convection. *Microvasc Res* **37**, 77–104.

[3] Heldin CH, Rubin K, Pietras K, and Östman A (2004). High interstitial fluid pressure—an obstacle in cancer therapy. *Nat Rev Cancer* **4**, 806–813.

[4] Jain RK and Gerlowski LE (1986). Extravascular transport in normal and tumor tissues. *Crit Rev Oncol Hematol* **5**, 115–170.

[5] Hofmann M, Guschel M, Bernd A, Bereiter-Hahn J, Kaufmann R, Tandi C, Wiig H, and Kippenberger S (2006). Lowering of tumor interstitial fluid pressure reduces tumor cell proliferation in a xenograft tumor model. *Neoplasia* **8**, 89–95.

[6] Hofmann M, Schultz M, Bernd A, Bereiter-Hahn J, Kaufmann R, and Kippenberger S (2007). Long-term lowering of tumor interstitial fluid pressure reduces Ki-67 expression. *J Biomech* **40**, 2324–2329.

[7] Hofmann M, McCormack E, Mujic M, Roßberg M, Bernd A, Bereiter-Hahn J, Gjertsen BT, Wiig H, and Kippenberger S (2009). Increased plasma colloid osmotic pressure facilitates the uptake of therapeutic macromolecules in a xenograft tumor model. *Neoplasia* **11**, 812–822.

[8] Wiig H, Reed RK, and Aukland K (1981). Micropuncture measurement of interstitial fluid pressure in rat subcutis and skeletal muscle: comparison to wick-in-needle technique. *Microvasc Res* **81**, 308–319.

[9] Wagner O, Schüler H, Hofmann P, Langer D, Dancker P, and Bereiter-Hahn J (2001). Sound attenuation of polymerizing actin reflects supramolecular structures: viscoelastic properties of actin gels modified by cytochalasin D, profilin and alpha-actinin. *J Biochem* **355**, 771–778.

[10] Litniewski J and Bereiter-Hahn J (1990). Measurements of cells in culture by scanning acoustic microscopy. *J Microsc* **158**, 95–107.

[11] Pflanzer R, Shelke A, Bereiter-Hahn J, Sader R, and Hofmann M (2012). Ultrasonic Quantification of Tumor Interstitial Fluid Pressure through Scanning Acoustic Microscopy. In: Nowicki A, Litniewski J, Kujawska T, editors. Acoustical Imaging, 31; 2012. p. 291–298.

[12] Bereiter-Hahn J, Karl I, Luers H, and Voth M (1995). Mechanical basis of cell shape: investigations with the scanning acoustic microscope. *Biochem Cell Biol* **73**, 337–348.

[13] Pflanzer R, Hofmann M, Shelke A, Habib A, Derwich W, Schmitz-Rixen T, Bernd A, Kaufmann R, and Bereiter-Hahn J (2014). Advanced 3D-sonographic imaging as a precise technique to evaluate tumor volume. *Transl Oncol* **7**, 681–686.

[14] Hompland T, Ellingsen C, Øvrebø KM, and Rofstad EK (2012). Interstitial fluid pressure and associated lymph node metastasis revealed in tumors by dynamic contrast-enhanced MR. *Cancer Res* **72**, 4899–4908.

[15] Wu M, Frieboes HB, McDougall SR, Chaplain MAJ, Cristini V, and Lowengrub J (2013). The effect of interstitial pressure on tumor growth: coupling with the blood and lymphatic vascular systems. *J Theor Biol* **320**, 131–151.

[16] Tadayyon H, Sadeghi-Naini A, and Czarnota GJ (2014). Noninvasive characterization of locally advanced breast cancer using textural analysis of quantitative ultrasound parametric images. *Transl Oncol* **7**, 759–767.